Geophysical Research Letters®

Key Points:

- When rain evaporation is removed in the PBL, convective self-aggregation (CSA) is triggered by convective heating of the moist regions
- Surprisingly, CSA only occurs when rain evaporation is almost totally removed in the PBL, due to opposing temperature and moisture effects
- CSA occurs more easily in a larger domain due to stronger radiatively induced subsidence, while cold pools play a less significant role

Correspondence to:

Y.-L. Hwong,
yiling.hwong@gmail.com

The Unreasonable Efficiency of Total Rain Evaporation Removal in Triggering Convective Self-Aggregation

Y.-L. Hwong[1] and C. J. Muller[1]

[1]Institute of Science and Technology Austria, Klosterneuburg, Austria

Abstract The elimination of rain evaporation in the planetary boundary layer (PBL) has been found to lead to convective self-aggregation (CSA) even without radiative feedback, but the precise mechanisms underlying this phenomenon remain unclear. We conducted cloud-resolving simulations with two domain sizes and progressively reduced rain evaporation in the PBL. Surprisingly, CSA only occurred when rain evaporation was almost completely removed. The additional convective heating resulting from the reduction of evaporative cooling in the moist patch was found to be the trigger, thereafter a dry subsidence intrusion into the PBL in the dry patch takes over and sets CSA in motion. Temperature and moisture anomalies oppose each other in their buoyancy effects, hence explaining the need for almost total rain evaporation removal. We also found radiative cooling and not cold pools to be the leading cause for the comparative ease of CSA to take place in the larger domain.

Plain Language Summary Convective clouds are not randomly scattered across the sky but tend to clump together, a phenomenon known as convective self-aggregation (CSA). The interaction between clouds and radiation is a key mechanism for CSA to occur. Curiously, CSA can still take place without this radiative feedback, provided that rain is prohibited from evaporating in the lowest layers of the atmosphere (~1 km), called the planetary boundary layer (PBL). To investigate the physical processes behind this type of CSA (no-evaporation CSA, or "NE-CSA"), we ran high resolution atmospheric model simulations and reduced rain evaporation in steps in the PBL. We found that the additional heat resulting from the reduction of evaporative cooling is crucial in triggering NE-CSA, thereafter the invasion of dry air into the PBL in the dry region takes over and intensifies aggregation. Surprisingly, allowing even a minuscule amount of rain to evaporate prevents NE-CSA from taking place. This is because removing rain evaporation has two opposing effects on convection: heating and drying. The former aids convection while the latter hinders it. Only when rain evaporation is almost completely eliminated can the heating effect be powerful enough to overcome the drying effect and kick-start NE-CSA.

1. Introduction

Convective self-aggregation (CSA), an atmospheric intrigue where deep convective clouds spontaneously organize into clusters under homogeneous radiative-convective equilibrium (RCE) conditions devoid of external forcing, has been extensively studied in cloud-resolving models (CRMs) (see Muller et al., 2022; Wing et al., 2018, for comprehensive reviews). These studies investigated myriad aspects of CSA in RCE, including its time and length scales (Patrizio & Randall, 2019; Wing & Cronin, 2016; Yanase et al., 2020), onset and maintenance mechanisms (Muller & Bony, 2015 [henceforth MB15]; Wing & Emanuel, 2014), impact on mean climate (Bretherton et al., 2005; Wing & Cronin, 2016) and climate sensitivity (Cronin & Wing, 2017; Wing, 2019; Wing et al., 2020), and relevance to tropical meteorology such as the Madden-Julian Oscillation (Arnold & Randall, 2015; Khairoutdinov & Emanuel, 2018) and tropical cyclones (Carstens & Wing, 2020; Muller & Romps, 2018). In CRM simulations, CSA has been found to manifest itself more readily in larger domains and coarser resolutions (Muller & Held, 2012; Yanase et al., 2020).

Radiative feedback has been found to be a crucial ingredient for CSA (MB15; Wing & Emanuel, 2014), while surface flux feedback is a favorable but not indispensable condition (Holloway & Woolnough, 2016; Muller & Held, 2012). The role of moisture has also been studied, including its effect on the dynamics of CSA (D. Yang, 2018a), the importance of dry-subsidence feedback in dry patch intensification (B. Yang & Tan, 2020), and the development of CSA through a moisture coarsening process (Craig & Mack, 2013; Windmiller & Craig, 2019). Generally, CSA has been associated with physical processes that generate a low-level circulation

leading to an upgradient transport of moist static energy (MSE) from dry to moist regions (Bretherton et al., 2005; Naumann et al., 2017; Yanase et al., 2022). However, the role of and precise mechanisms producing this circulation remain ambiguous: shallow circulation has been argued to hamper CSA from developing in smaller domains (Jeevanjee & Romps, 2013); its strength and importance have been found to be model dependent (Cerlini et al., 2023); questions also remain whether it is radiatively (Muller & Held, 2012; Naumann et al., 2017) or convectively driven (Holloway & Woolnough, 2016).

Rain evaporation has also been found to impact CSA. When rain evaporation is disabled in the PBL, CSA can occur even in the absence of radiative and surface flux feedbacks (Holloway & Woolnough, 2016; MB15; D. Yang, 2019). The physical mechanisms underlying this type of CSA—referred to here as "no-evaporation CSA" (NE-CSA)—is still unclear and is the focus of this study. Several processes have been proposed to be responsible for NE-CSA. MB15 referred to NE-CSA as "moisture-memory aggregation" and suggested that the feedback between clouds and the environmental water vapor potentially underlies this type of aggregation. Another process known to affect convective organization is entrainment (Mapes & Neale, 2011; Tompkins, 2001; Tompkins & Semie, 2017): the entrainment of dry air hinders convection by diluting the plume's MSE (and thus buoyancy during subsequent ascent), representing a positive feedback that could organize convection into clusters. However, D. Yang (2019) showed that NE-CSA can still occur without entrainment-related feedback. Instead, the author proposed that the convective heating-overturning circulation (CHOC) feedback is responsible for generating the available potential energy (APE) necessary for NE-CSA to develop.

Another hypothesis for NE-CSA relates to cold pools, which many studies have shown to hinder CSA (Nissen & Haerter, 2021; Yanase et al., 2020). Jeevanjee and Romps (2013) showed that convection always self-aggregated regardless of domain sizes when rain evaporation was removed in the lowest 1 km. The authors hypothesized that cold pools inhibit CSA by homogenizing the PBL properties between dry and moist areas. Eliminating cold pools hence eased the occurrence of CSA. However, D. Yang (2018a) used scale analyses to show that cold pools are not the reason for NE-CSA but the decrease in evaporative cooling and associated increase in APE is the likelier cause.

Given the lack of consensus in this area, the goal of our study is to investigate the mechanisms underlying NE-CSA. Building on the experiments of D. Yang (2018a), but instead of completely removing rain evaporation in the PBL—which represents a dramatic perturbation to the system—we progressively reduced rain evaporation and observed the impact on CSA. Our research questions are:

1. How does CSA change when rain evaporation is reduced in the PBL?
2. Which physical processes are involved in the development of CSA when rain evaporation is reduced or removed in the PBL?

2. Methods

2.1. Model and Simulation Setup

We performed 3-D simulations with the System for Atmosphere Modeling (SAM) CRM (version 6.10.8; Khairoutdinov & Randall, 2003). SAM solves the anelastic conservation equations of momentum, mass, energy and water. Non-rotating RCE simulations over an ocean surface were conducted, with a constant sea-surface temperature of 301 K. Diurnal cycle was disabled by setting the solar constant and zenith angle to values of 685 W m^{-2} and 51.7° (following Tompkins & Craig, 1998), respectively. To focus on the rain evaporation feedback, we disabled radiative and surface flux feedbacks by horizontally homogenizing them at every time step (additional results with interactive radiation and surface fluxes are included in Supporting Information S1). The SAM one-moment microphysics parameterization was used. Two domain sizes were tested: 128×128 km ($\Delta x = 1$ km; denoted as L128) and 256×256 km ($\Delta x = 4$ km; L256). A 64-level stretched vertical grid was used, with the model bottom and top at 37.5 m and 27 km, respectively. A sponge layer with Newtonian relaxation to no motion was applied in the top third of the domain to avoid unrealistic gravity wave build-up. All simulations were run for 40 days.

2.2. Rain Evaporation Reduction

Following MB15, we changed the amount of rain evaporation by multiplying the evaporation of precipitating water by a factor of α in the lowest 1 km. We first conducted a set of experiments where rain evaporation was

progressively reduced in steps of α = [0.8, 0.6, 0.4, 0.2, 0]. Surprisingly, we found that convection became disaggregated even at α = 0.2. Further reduction of rain evaporation showed that CSA only occurred when rain evaporation was almost completely removed. The α values for convection to transition from a scattered to an aggregated state were smaller for L128 than L256 by around an order of magnitude. In view of this, we conducted a new set of experiments by setting α = [0.05, 0.02, 0.01, 0.005, 0.002, 0.001, 0] for L128 and α = [0.5, 0.2, 0.1, 0.05, 0.02, 0.01, 0] for L256. Control experiments with α = 1 were also conducted. All experimental configurations are listed in Table S1 in Supporting Information S1.

2.3. Buoyancy Analyses

A high (low) surface pressure anomaly of the dry (moist) patch and the associated buoyancy anomalies are necessary to establish a shallow circulation frequently linked to CSA (Shamekh et al., 2020; D. Yang, 2018a). Assuming a weak temperature (and buoyancy) gradient (WTG) in the free troposphere (FT) (Sobel et al., 2001), our analyses focus primarily on the generation of buoyancy anomalies in the PBL and the physical processes that could amplify these anomalies. Following D. Yang (2018a), we used virtual potential temperature as a proxy for buoyancy as related by

$$b = g\frac{\theta_v'}{\overline{\theta_v}} \approx g\left(\frac{\theta'}{\overline{\theta}} + \frac{\epsilon q_v'}{1 + \overline{q_v}}\right) \tag{1}$$

where b is the buoyancy, g the gravitational acceleration, θ_v' and θ' the virtual potential temperature and potential temperature anomalies (deviation from domain mean), respectively, q_v' the water vapor specific humidity anomaly, and ϵ is $M_{air}/M_{h2o} - 1 = 0.61$. Overbars indicate domain mean values. Equation 1 implies that anomalous warming (cooling) and moistening (drying) can both be a source (sink) of buoyancy. Rain evaporation is a source of evaporative cooling and moistening, representing two opposing effects on buoyancy. To investigate which effect is dominant in NE-CSA we analyzed the temperature and moisture anomaly terms in Equation 1 separately.

3. Results

3.1. Convective Self-Aggregation and Cold Pools

Figure 1 shows the aggregation state of selected α cases and their associated cold pools. We show snapshots of precipitable water (PW) at the end of the simulations as an indicator of aggregation, as PW variance has been shown to increase dramatically when convection self-aggregates (Arnold & Randall, 2015; Bretherton et al., 2005). We use the virtual potential temperature anomaly (deviation from domain mean) at the lowest model level as a proxy for cold pools, following Kurowski et al. (2018). Consistent with previous findings, convection does not self-aggregate when rain evaporation is present (α = 1) but does so when it is completely removed (α = 0). Unexpectedly, this aggregation is found to be very singular for near zero α values. The precise threshold depends somewhat on the domain size. For the larger domain the α value for convection to transition from a scattered to an aggregated state is larger: when α was decreased from 0.01 to 0.005 for L128 (Figures 1b and 1c) and from 0.1 to 0.05 for L256 (Figures 1j and 1k).

Interestingly, cold pools are largely absent at these α values for both domains (Figures 1f and 1g for L128; Figures 1n and 1o, for L256), albeit for L256 there might be very weak cold pools for α = 0.1. Contrary to what previous studies have found—where convection self-aggregates at all domain sizes in the absence of cold pools— our results suggest that, although they play an important role, cold pools alone cannot explain NE-CSA: convection sometimes does not self-aggregate even in the absence of cold pools. In short, the markedly different aggregation degrees observed are not always accompanied by similarly distinct cold pool strengths. We further observed a quicker CSA development in the smaller domain size. For L128, CSA onset occurred by around day-5 (stabilization around day-20) and for L256 by around day-10 (stabilization around day-30; Figure S1 in Supporting Information S1).

We further note that allowing radiative and surface flux feedbacks and changing the height over which rain evaporation is removed do not dramatically alter the α values for CSA to occur in L128 (Text S1, Figures S2 and S3 in Supporting Information S1).
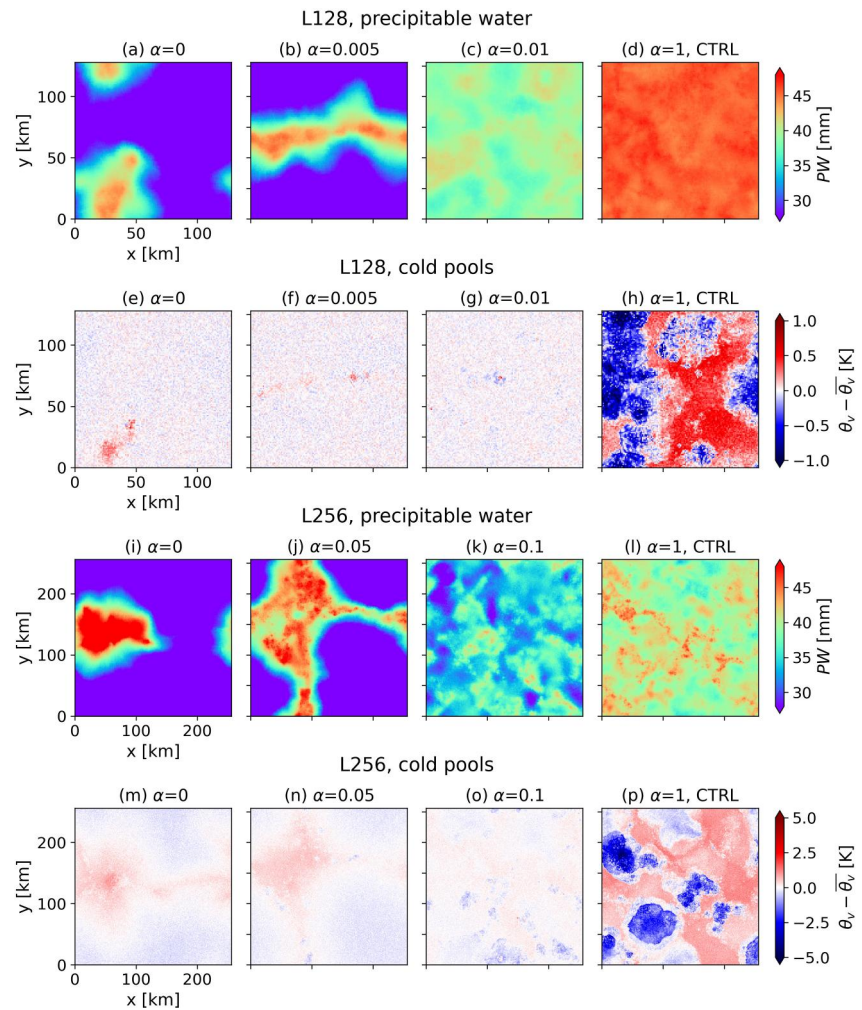
Figure 1. Snapshots at the end of the 40-day simulations of PW and virtual potential temperature anomaly (cold pools) for (a–h) L128 and (i–p) L256.

3.2. Shallow Circulation

It is as yet unclear whether a low-level circulation—a common feature of the conventional radiatively driven aggregation (RDA)—would also be present in NE-CSA. A recent study has found that CSA can still develop without a shallow circulation when the subcloud layer is close to saturation (Cerlini et al., 2023), which would prevent precipitation from evaporating, analogous to NE-CSA. To observe the circulation fields we show the MSE and stream function Ψ ranked by column relative humidity (CRH) averaged over the final 5 days in Figure 2 for selected α cases (see Bretherton et al., 2005, for computation details of Ψ). A low-level circulation is indeed present for the aggregated but not the scattered cases. This circulation is characterized by a near surface outflow from dry to moist regions, and a partial return flow above the PBL ($\sim$2–3 km). The outflow air has higher MSE compared to the return flow, resulting in an enhanced MSE gradient that over time renders the dry regions drier and moist regions moister. The circulation fields of the aggregated cases also show an intrusion of dry subsidence air from the FT into the PBL (below 1 km) in the driest blocks and an accompanying upward motion in the moistest regions.

3.3. Convectively Driven Aggregation

Spatial contrasts in radiative cooling in the PBL are believed to be a driving force of the shallow circulation between dry and moist regions (MB15; Naumann et al., 2017). What, then, generates the shallow circulation in NE-CSA where radiation is horizontally homogenized? To investigate this, we compute θ'_v as a proxy for
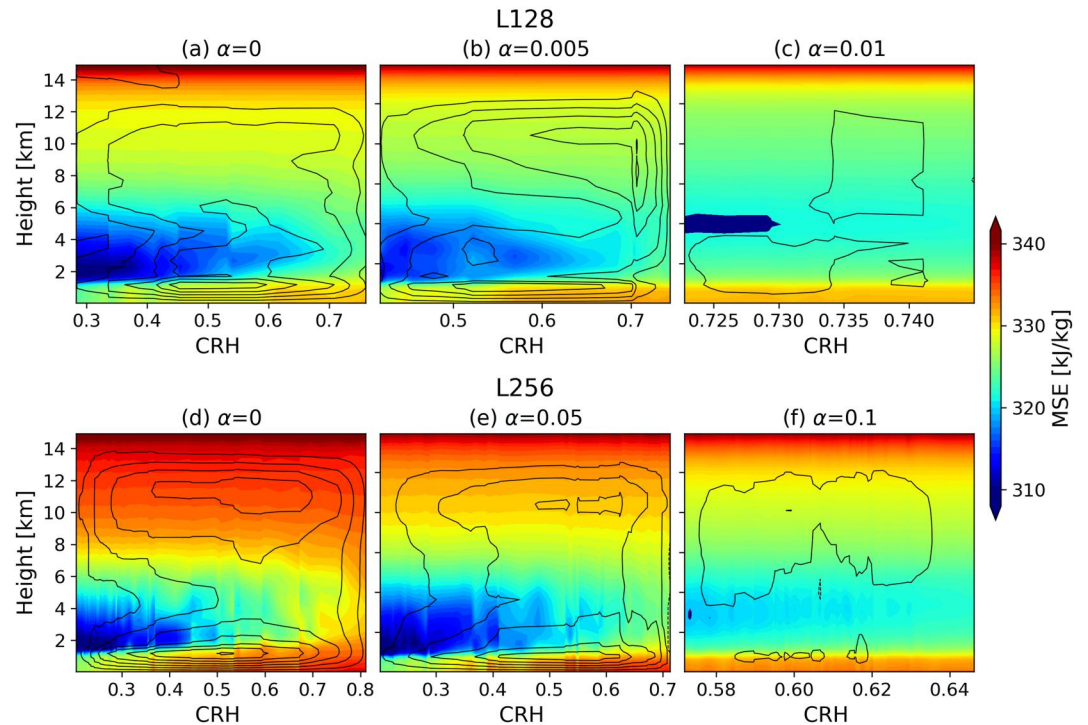
Figure 2. MSE (shading) and stream functions (black contours counterclockwise, intervals of 0.02 kg m^{-2} s^{-1} for L128 and 0.04 kg m^{-2} s^{-1} for L256) averaged over the final 5 days for the aggregated (a, b, d, e) and scattered (c, f) cases.

buoyancy, as a positive buoyancy gradient between the dry and moist areas has been shown to be a prerequisite for low-level circulations to develop (Yanase et al., 2022). We show in Figure 3 the time-series of θ'_v and the contributions of θ' and q'_v (calculated following Equation 1), vertically averaged over the lowest 1 km and for the dry and moist patches separately. Note that θ'_v is very small in the FT, consistent with the WTG assumption (Figure S4 in Supporting Information S1). We define dry and moist regions as grid points where PW is below the 10th and above the 90th percentiles, respectively.

We first describe the overall θ'_v trends. To establish a positive buoyancy gradient, θ'_v of the moist patch must be greater than that of the dry patch. For the aggregated cases, this is indeed observed for both domains and throughout the simulation period (Figure 3a), indicating a consistent high pressure anomaly in the PBL dry patch (negative $\theta'_{v,\mathrm{dry}}$), generating an outflow that is conducive to shallow circulation development as discovered by Yanase et al. (2022). In contrast, for the non-aggregated cases (Figure 3d) the moist patch is either negatively (L256) or very weakly positively buoyant (L128), with very small θ'_v's that have a diminishing probability of persistence, evident in the intermittent zero values displayed. This suggests that a large enough positive buoyancy gradient that continuously develops is necessary for aggregation to occur, that is, both the magnitude of $\Delta\theta'_v$ between the dry and moist patches and its persistence in time matter.

Next we analyze the θ' and q'_v time-series of the aggregated cases. There appears to be three phases in the development of NE-CSA: triggering, intensification, and stabilization. Since radiation and surface fluxes are homogenized, we focus on convective processes, whose effects are more prominent in the moist patch. During the triggering phase (initial period when the moist patch temperature $[\theta'_{\mathrm{moist}}]$ and moisture $[q'_{v,\mathrm{moist}}]$ effects oppose each other: day 0–3 for L128; day 0–7 for L256), the effect of rain evaporation removal is most evident: a reduction in evaporative cooling and moistening results in a net increase in convective heating and drying of the moist patch (positive θ'_{dry} and negative $q'_{v,\mathrm{moist}}$ in Figures 3b and 3c). Although these are two opposing buoyancy effects, the heating effect prevails, resulting in a positive $\theta'_{v,\mathrm{moist}}$. This indicates that in the triggering phase the additional convective heating of the moist patch (latent heat release from condensation) plays an important role in
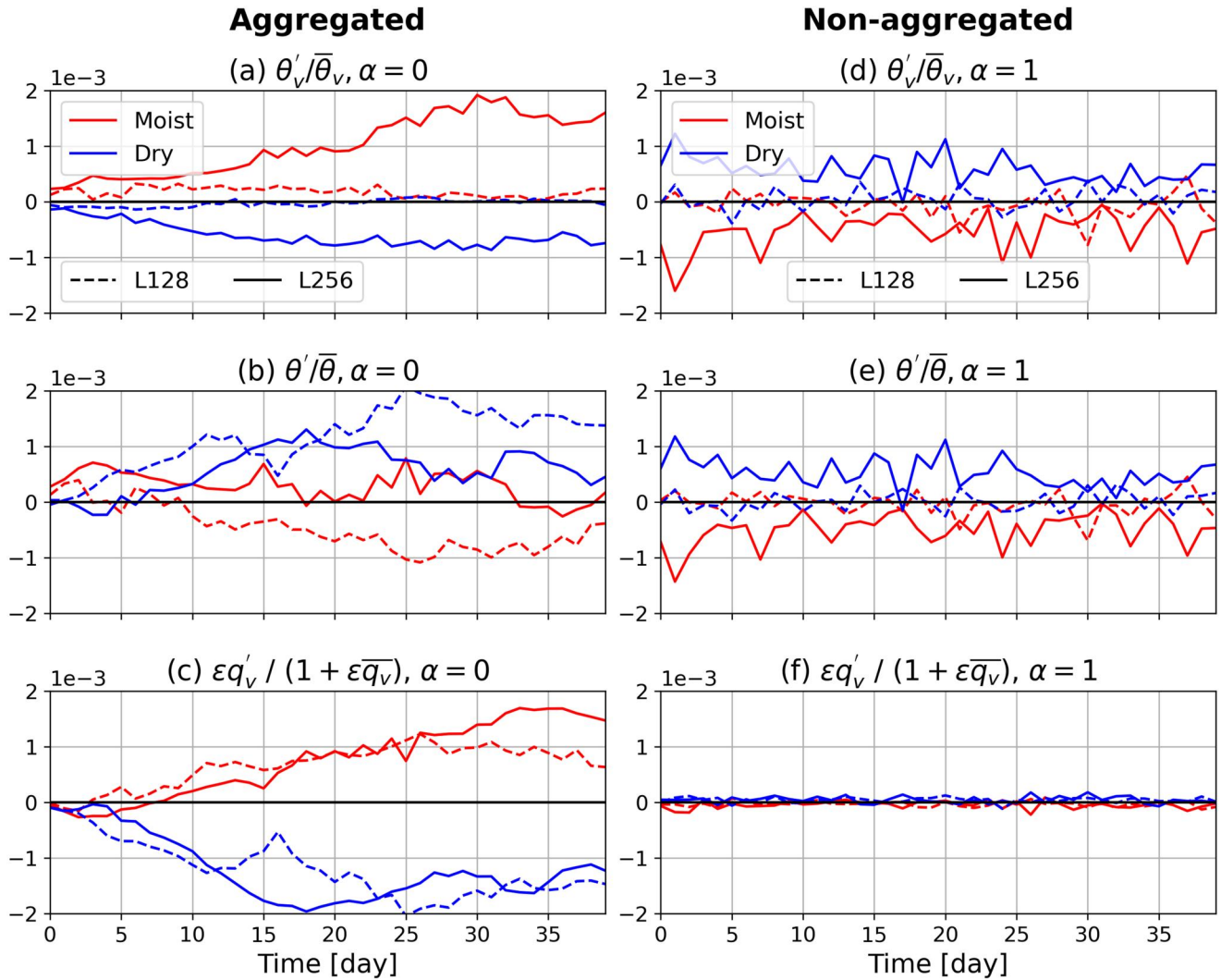
Figure 3. Time evolution of θ'_v (top row) and the contributions of θ' (middle row) and q'_v (bottom row) of the (a–c) aggregated and (d–f) non-aggregated cases.

kick-starting NE-CSA. For the scattered cases (Figures 3e and 3f), there is insufficient reduction in evaporative cooling for convective heating to set-off CSA.

During the intensification phase (when $q'_{v,\mathrm{dry}}$ is decreasing after the triggering phase: day 3–10 for L128, day 7–17 for L256), the q'_v effects dominate the trend in buoyancy (θ'_v). A gradual decrease (increase) in $q'_{v,\mathrm{dry}}$ ($q'_{v,\mathrm{moist}}$) is observed (Figure 3c). This is indicative of the intrusion of dry (dense) air from the FT into the PBL in the dry patch, which causes the decreasing buoyancy in the dry patch PBL, resulting in a divergent flow from it. Crucially, the virtual effect of subsidence drying exceeds subsidence warming (the overall negative $\theta'_{v,\mathrm{dry}}$ indicates $q'_{v,\mathrm{dry}}$ dominates over θ'_{dry}), maintaining the negative buoyancy anomaly of the dry patch. This is reminiscent of the "dry-subsidence feedback" postulated by B. Yang and Tan (2020) (further analyses of the dry-subsidence feedback is presented in Text S2 and Figure S5 in Supporting Information S1). In short, after a sufficiently strong ignition from convective heating in the triggering phase, the virtual effect takes over to intensify CSA. For the scattered case this take-over of virtual effect failed to materialize (Figure 3f) due to weak ignition during the triggering phase.

After the intensification period NE-CSA enters the mature phase (when $q'_{v,\mathrm{moist,dry}}$ stabilizes: after day-10 for L128, after day-17 for L256). A competing effect between θ' and q'_v is observed: the virtual effect aids CSA while θ' contribution opposes it. For both domains the θ' contribution causes the dry patch to be positively
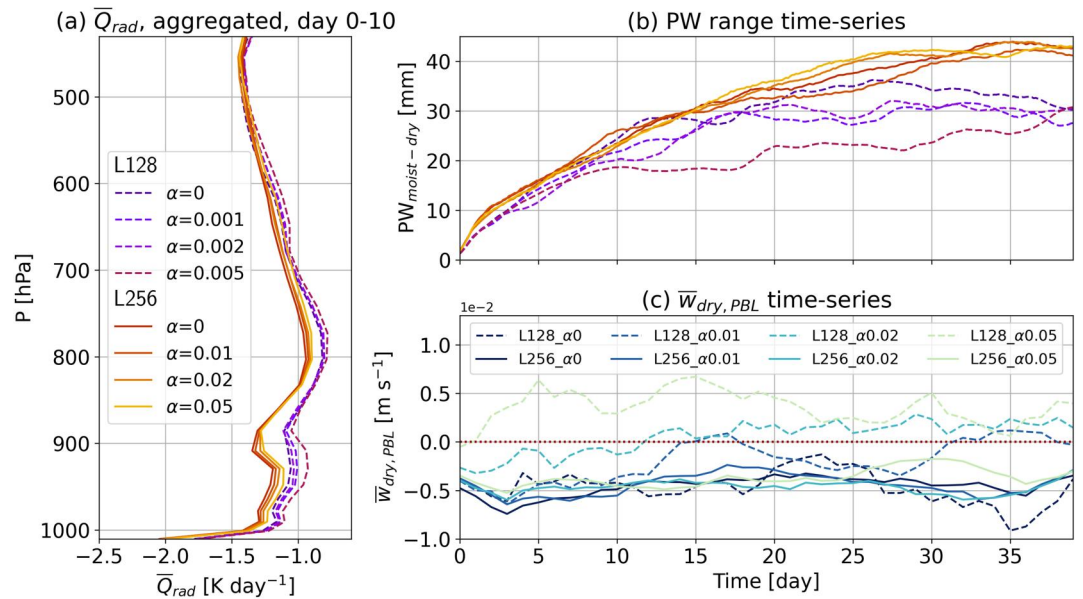
Figure 4. (a) Domain- and time-averaged (first 10-day) profiles of $\overline{Q}_{rad}$ and (b) PW range time-series of the aggregated cases, (c) $\overline{w}_{dry,PBL}$ time-series.

buoyant, and the moist patch to be negatively buoyant for L128 from day-10 onwards and trend toward negative buoyancy for L256 (Figure 3b). Time-series of vertical velocity indicates that the positive θ'_{dry} is probably due to subsidence warming (Figures S5a and S5d in Supporting Information S1) while the cooling of the moist patch could be due to breakthrough evaporative cooling from the FT ($\overline{T}_{PBL,moist}$ gradually decreases, see Figure S6 in Supporting Information S1). This competing θ' and q'_v effect explains the need for an almost total removal of rain evaporation in the PBL to, firstly, supply a strong enough boost in the triggering phase, and secondly, to counter the effect of evaporative cooling and ensure $\theta'_{v,moist}$ remains positive in the mature phase.

The process described above is consistently observed across different α's (Figures S7 and S8 in Supporting Information S1) and is markedly different from the mechanisms underlying RDA (Text S3, Figure S9 in Supporting Information S1). Additionally, NE-CSA does not exhibit hysteresis: reintroducing rain evaporation in a simulation restarted from an aggregated state quickly resulted in disaggregation.

3.4. Domain Size and Radiative Cooling

As investigating the domain size sensitivity of NE-CSA is beyond the scope of this study, we only tested two domain sizes. Nonetheless, the large difference in α threshold for NE-CSA to occur in the two domains is intriguing. We show in Figure 4 the domain- and time-averaged (first 10-day) radiative cooling profiles $\left(\overline{Q}_{rad}\right)$ of the aggregated cases, time-series of the PW difference between moist and dry patches and dry region vertical velocity (averaged over lowest 1 km). Studies have found cloud-radiative feedback to be an important factor contributing to the domain size dependence of CSA (MB15; Muller & Held, 2012). We found $\overline{Q}_{rad}$ to be generally stronger for L256 than L128. This suggests that—even in the absence of spatial inhomogeneity—the magnitude of $\overline{Q}_{rad}$ still matters for NE-CSA. We postulate that this is due to the stronger subsidence in the dry region induced by a stronger $\overline{Q}_{rad}$. We confirmed this with sensitivity runs imposing the radiative cooling of the large domain in the small domain and vice versa: stronger radiative cooling, even homogenized, was found to favor aggregation. The range of PW increases with domain size (Figure 4b): the driest region is drier in L256 than L128 when aggregation is starting to occur, hence a stronger subsidence is generated. This enables the free-tropospheric dry air to more easily enter the PBL, hence permitting a higher α threshold in L256. This hypothesis also explains why convection self-aggregates in L256 but not L128 for the same α's (0.01, 0.02, 0.05), with similar cold pool strengths in both domains: subsidence is larger for the larger domain ($\overline{w}_{dry,PBL}$ more negative; Figure 4c).

Nonetheless, subsidence alone cannot explain the propensity for aggregation. A strong convective heating is still needed to kick-start aggregation. For example, L128_α0 and L128_α0.01 display similar subsidence trajectory in the first 10 days, but aggregation already took off by day-5 for the former while the latter remains non-aggregated (Figure S1 in Supporting Information S1), indicating that the ignition from convective heating (determined by α) was insufficient for L128_α0.01. In summary, larger domains generally produce stronger subsidence, and provided sufficient initial boost from convective heating in the moist region, free-tropospheric dry air will enter the PBL in the dry region and CSA will take off.

4. Conclusions

We investigate the physical mechanisms underlying convective self-aggregation (CSA) in the absence of radiative and surface flux feedbacks and with rain evaporation removed or reduced in the PBL, referred to here as no-evaporation CSA (NE-CSA). We progressively reduced rain evaporation by multiplying it by a factor α. We tested two domain sizes: 128×128 km (L128) and 256×256 km (L256).

Our main finding is that NE-CSA only occurs when rain evaporation is entirely (or almost entirely) removed. This is because the temperature and moisture impacts of evaporation reduction oppose each other, making this feedback very sensitive: only when rain evaporation is almost completely removed ($\alpha \approx 0$) can the additional heating trigger aggregation. This net increase in heating is a result of sufficient reduction in evaporative cooling that enables latent heating to dominate. The resulting buoyancy anomalies between the dry and moist patch can induce a shallow circulation even without the help of radiative and surface flux feedbacks, echoing the mechanisms underlying the shallow cumulus aggregation of Bretherton and Blossey (2017). Once the initial spark renders the moist patch positively buoyant enough to kick-start CSA, the virtual effect takes over, whereby free-tropospheric dry subsidence descends into the PBL of the dry region and sets CSA in motion. In the mature phase the positive contribution of q'_v effects (subsidence drying of dry patch; moisture convergence into moist patch) is counteracted by the negative contribution of θ' effects (subsidence warming of dry patch; evaporative cooling of moist patch), hence also explaining the need for small α's to attenuate this negative θ' effect. Importantly, these findings also apply in more realistic setups with interactive radiation and surface fluxes, and with rain evaporation removed over different PBL heights, indicating the relevance of our experiments in isolating the effects of rain evaporation in CSA.

The above findings are consistent with the results of D. Yang (2018a, 2018b) on the importance of evaporative cooling and PBL diabatic processes in influencing CSA. The crucial difference of our study is the inclusion of small but non-zero α values to mimic more realistic atmospheric scenarios and the discovery of the resultant disintegration of CSA, lending important nuances to the interpretation of studies implementing a total removal of rain evaporation.

In contrast to the dry patch-driven radiatively driven aggregation (RDA), in NE-CSA the moist and dry regions work in tandem: heating of the moist patch provides the spark to trigger aggregation and subsidence in the dry patch supplies the boost that eventually sets off a shallow circulation that sustains CSA. Given the crucial role of convective heating (reminiscent of the CHOC feedback proposed by D. Yang (2019)), we suggest that this type of aggregation should be more appropriately referred to as convectively driven aggregation (CDA) instead of "moisture-memory aggregation." We also observed that CDA develops significantly quicker than RDA, due to convection being a faster process than radiation.

Further, we found that CDA was able to occur at larger α thresholds in L256 than L128 and cold pools alone cannot explain this domain size dependence, unlike what was suggested in earlier studies. Instead, we postulate that the broadening of the PW range and concomitant increase in radiative cooling is the likelier cause for the relative ease of CDA to occur in the larger domain. The stronger subsidence induced hence allows for a comparatively smaller reduction in evaporative cooling.

Our study expands established theories about CSA, which have predominantly focused on the mechanisms underlying dry patch expansion. By illuminating the role of convective heating, we think that the physical processes in the moist patch are also worthy of note and should be taken into account when considering the numerous environmental conditions under which aggregation can occur.

Data Availability Statement

The data, scripts and model source codes and files required to reproduce the results described in this manuscript are available in Hwong and Muller (2023).

References

Arnold, N. P., & Randall, D. A. (2015). Global-scale convective aggregation: Implications for the Madden-Julian oscillation. *Journal of Advances in Modeling Earth Systems*, *7*(4), 1499–1518. https://doi.org/10.1002/2015ms000498

Bretherton, C. S., & Blossey, P. (2017). Understanding mesoscale aggregation of shallow cumulus convection using large-eddy simulation. *Journal of Advances in Modeling Earth Systems*, *9*(8), 2798–2821. https://doi.org/10.1002/2017ms000981

Bretherton, C. S., Blossey, P. N., & Khairoutdinov, M. (2005). An energy-balance analysis of deep convective self-aggregation above uniform SST. *Journal of the Atmospheric Sciences*, *62*(12), 4273–4292. https://doi.org/10.1175/jas3614.1

Carstens, J. D., & Wing, A. A. (2020). Tropical cyclogenesis from self-aggregated convection in numerical simulations of rotating radiative-convective equilibrium. *Journal of Advances in Modeling Earth Systems*, *12*(5), e2019MS002020. https://doi.org/10.1029/2019ms002020

Cerlini, P. B., Saraceni, M., & Silvestri, L. (2023). Competing effect of radiative and moisture feedback in convective aggregation states in two CRMS. *Journal of Advances in Modeling Earth Systems*, *15*(2), e2022MS003323. https://doi.org/10.1029/2022ms003323

Craig, G. C., & Mack, J. M. (2013). A coarsening model for self-organization of tropical convection. *Journal of Geophysical Research: Atmospheres*, *118*(16), 8761–8769. https://doi.org/10.1002/jgrd.50674

Cronin, T. W., & Wing, A. A. (2017). Clouds, circulation, and climate sensitivity in a radiative-convective equilibrium channel model. *Journal of Advances in Modeling Earth Systems*, *9*(8), 2883–2905. https://doi.org/10.1002/2017ms001111

Holloway, C. E., & Woolnough, S. J. (2016). The sensitivity of convective aggregation to diabatic processes in idealized radiative-convective equilibrium simulations. *Journal of Advances in Modeling Earth Systems*, *8*(1), 166–195. https://doi.org/10.1002/2015ms000511

Hwong, Y.-L., & Muller, C. (2023). Data - The unreasonable efficiency of total rain evaporation removal in triggering convective self-aggregation (version 5) [Dataset]. Zenodo. https://doi.org/10.5281/zenodo.10687169

Jeevanjee, N., & Romps, D. M. (2013). Convective self-aggregation, cold pools, and domain size. *Geophysical Research Letters*, *40*(5), 994–998. https://doi.org/10.1002/grl.50204

Khairoutdinov, M. F., & Emanuel, K. (2018). Intraseasonal variability in a cloud-permitting near-global equatorial aquaplanet model. *Journal of the Atmospheric Sciences*, *75*(12), 4337–4355. https://doi.org/10.1175/jas-d-18-0152.1

Khairoutdinov, M. F., & Randall, D. A. (2003). Cloud resolving modeling of the arm summer 1997 IOP: Model formulation, results, uncertainties, and sensitivities. *Journal of the Atmospheric Sciences*, *60*(4), 607–625. https://doi.org/10.1175/1520-0469(2003)060<0607:crmota>2.0.co;2

Kurowski, M. J., Suselj, K., Grabowski, W. W., & Teixeira, J. (2018). Shallow-to-deep transition of continental moist convection: Cold pools, surface fluxes, and mesoscale organization. *Journal of the Atmospheric Sciences*, *75*(12), 4071–4090. https://doi.org/10.1175/jas-d-18-0031.1

Mapes, B., & Neale, R. (2011). Parameterizing convective organization to escape the entrainment dilemma. *Journal of Advances in Modeling Earth Systems*, *3*(2). https://doi.org/10.1029/2011ms000042

Muller, C., & Bony, S. (2015). What favors convective aggregation and why? *Geophysical Research Letters*, *42*(13), 5626–5634. https://doi.org/10.1002/2015gl064260

Muller, C., & Held, I. M. (2012). Detailed investigation of the self-aggregation of convection in cloud-resolving simulations. *Journal of the Atmospheric Sciences*, *69*(8), 2551–2565. https://doi.org/10.1175/jas-d-11-0257.1

Muller, C., & Romps, D. M. (2018). Acceleration of tropical cyclogenesis by self-aggregation feedbacks. *Proceedings of the National Academy of Sciences of the United States of America*, *115*(12), 2930–2935. https://doi.org/10.1073/pnas.1719967115

Muller, C., Yang, D., Craig, G., Cronin, T., Fildier, B., Haerter, J. O., et al. (2022). Spontaneous aggregation of convective storms. *Annual Review of Fluid Mechanics*, *54*(1), 133–157. https://doi.org/10.1146/annurev-fluid-022421-011319

Naumann, A. K., Stevens, B., Hohenegger, C., & Mellado, J. P. (2017). A conceptual model of a shallow circulation induced by prescribed low-level radiative cooling. *Journal of the Atmospheric Sciences*, *74*(10), 3129–3144. https://doi.org/10.1175/jas-d-17-0030.1

Nissen, S. B., & Haerter, J. O. (2021). Circling in on convective self-aggregation. *Journal of Geophysical Research: Atmospheres*, *126*(20), e2021JD035331. https://doi.org/10.1029/2021jd035331

Patrizio, C. R., & Randall, D. A. (2019). Sensitivity of convective self-aggregation to domain size. *Journal of Advances in Modeling Earth Systems*, *11*(7), 1995–2019. https://doi.org/10.1029/2019ms001672

Shamekh, S., Muller, C., Duvel, J.-P., & d'Andrea, F. (2020). Self-aggregation of convective clouds with interactive sea surface temperature. *Journal of Advances in Modeling Earth Systems*, *12*(11), e2020MS002164. https://doi.org/10.1029/2020ms002164

Sobel, A. H., Nilsson, J., & Polvani, L. M. (2001). The weak temperature gradient approximation and balanced tropical moisture waves. *Journal of the Atmospheric Sciences*, *58*(23), 3650–3665. https://doi.org/10.1175/1520-0469(2001)058<3650:twtgaa>2.0.co;2

Tompkins, A. M. (2001). Organization of tropical convection in low vertical wind shears: The role of water vapor. *Journal of the Atmospheric Sciences*, *58*(6), 529–545. https://doi.org/10.1175/1520-0469(2001)058<0529:ootcil>2.0.co;2

Tompkins, A. M., & Craig, G. C. (1998). Radiative–convective equilibrium in a three-dimensional cloud-ensemble model. *Quarterly Journal of the Royal Meteorological Society*, *124*(550), 2073–2097. https://doi.org/10.1256/smsqj.55012

Tompkins, A. M., & Semie, A. G. (2017). Organization of tropical convection in low vertical wind shears: Role of updraft entrainment. *Journal of Advances in Modeling Earth Systems*, *9*(2), 1046–1068. https://doi.org/10.1002/2016ms000802

Windmiller, J. M., & Craig, G. C. (2019). Universality in the spatial evolution of self-aggregation of tropical convection. *Journal of the Atmospheric Sciences*, *76*(6), 1677–1696. https://doi.org/10.1175/jas-d-18-0129.1

Wing, A. A. (2019). Self-aggregation of deep convection and its implications for climate. *Current Climate Change Reports*, *5*, 1–11. https://doi.org/10.1007/s40641-019-00120-3

Wing, A. A., & Cronin, T. W. (2016). Self-aggregation of convection in long channel geometry. *Quarterly Journal of the Royal Meteorological Society*, *142*(694), 1–15. https://doi.org/10.1002/qj.2628

Wing, A. A., Emanuel, K., Holloway, C. E., & Muller, C. (2018). Convective self-aggregation in numerical simulations: A review. In *Shallow clouds, water vapor, circulation, and climate sensitivity* (pp. 1–25).

Wing, A. A., & Emanuel, K. A. (2014). Physical mechanisms controlling self-aggregation of convection in idealized numerical modeling simulations. *Journal of Advances in Modeling Earth Systems*, *6*(1), 59–74. https://doi.org/10.1002/2013ms000269

Wing, A. A., Stauffer, C. L., Becker, T., Reed, K. A., Ahn, M.-S., Arnold, N. P., et al. (2020). Clouds and convective self-aggregation in a multimodel ensemble of radiative-convective equilibrium simulations. *Journal of Advances in Modeling Earth Systems*, *12*(9), e2020MS002138. https://doi.org/10.1029/2020ms002138

Yanase, T., Nishizawa, S., Miura, H., Takemi, T., & Tomita, H. (2020). New critical length for the onset of self-aggregation of moist convection. *Geophysical Research Letters*, *47*(16), e2020GL088763. https://doi.org/10.1029/2020gl088763

Yanase, T., Nishizawa, S., Miura, H., Takemi, T., & Tomita, H. (2022). Low-level circulation and its coupling with free-tropospheric variability as a mechanism of spontaneous aggregation of moist convection. *Journal of the Atmospheric Sciences*, *79*(12), 3429–3451. https://doi.org/10.1175/jas-d-21-0313.1

Yang, B., & Tan, Z.-M. (2020). The initiation of dry patches in cloud-resolving convective self-aggregation simulations: Boundary layer dry-subsidence feedback. *Journal of the Atmospheric Sciences*, *77*(12), 4129–4141. https://doi.org/10.1175/jas-d-20-0133.1

Yang, D. (2018a). Boundary layer diabatic processes, the virtual effect, and convective self-aggregation. *Journal of Advances in Modeling Earth Systems*, *10*(9), 2163–2176. https://doi.org/10.1029/2017ms001261

Yang, D. (2018b). Boundary layer height and buoyancy determine the horizontal scale of convective self-aggregation. *Journal of the Atmospheric Sciences*, *75*(2), 469–478. https://doi.org/10.1175/jas-d-17-0150.1

Yang, D. (2019). Convective heating leads to self-aggregation by generating available potential energy. *Geophysical Research Letters*, *46*(17–18), 10687–10696. https://doi.org/10.1029/2019gl083805

References From the Supporting Information

Bretherton, C. S., & Smolarkiewicz, P. K. (1989). Gravity waves, compensating subsidence and detrainment around cumulus clouds. *Journal of the Atmospheric Sciences*, *46*(6), 740–759. https://doi.org/10.1175/1520-0469(1989)046<0740:gwcsad>2.0.co;2

Lorenz, E. N. (1955). Available potential energy and the maintenance of the general circulation. *Tellus*, *7*(2), 157–167. https://doi.org/10.3402/tellusa.v7i2.8796

Yang, D., Zhou, W., & Seidel, S. D. (2022). Substantial influence of vapour buoyancy on tropospheric air temperature and subtropical cloud. *Nature Geoscience*, *15*(10), 781–788. https://doi.org/10.1038/s41561-022-01033-x